High-temperature neutron diffraction and the temperature-dependent crystal structures of the *MAX* phases Ti_3SiC_2 and Ti_3GeC_2

Nina J. Lane,[1] Sven C. Vogel,[2] and Michel W. Barsoum[1]
[1]*Department of Materials Science and Engineering, Drexel University, Philadelphia, Pennsylvania 19104, USA*
[2]*Los Alamos Neutron Science Center, Los Alamos National Laboratory, Los Alamos, New Mexico 87545, USA*
(Received 2 August 2010; revised manuscript received 6 October 2010; published 10 November 2010)

Herein, we report on the crystal structures of the isostructural Ti_3SiC_2 and Ti_3GeC_2 phases determined by Rietveld analysis of neutron diffraction data in the 100° to 1100 °C temperature range. The results show that the Si and Ge atoms vibrate anisotropically with the highest amplitudes and within the basal planes. The equivalent isotropic thermal motion behavior does not differ significantly between the two phases; the anisotropic thermal motion, interatomic distances, and bond angles, however, show strikingly different behavior. Furthermore, while the Ti-Si bonds increase linearly with increasing temperature, the Ti-Ge bonds apparently do not. The anisotropic motion of the Ge atoms in the basal plane with the correlated motion between the Ti and the Ge atoms is invoked as a possible explanation. The volume expansions are $9.0(\pm0.1)\times10^{-6}$ K^{-1} and $8.7(\pm0.1)\times10^{-6}$ K^{-1} for Ti_3SiC_2 and Ti_3GeC_2, respectively; the expansions along the *a* and *c* axes are $\alpha_a=8.9(\pm0.1)\times10^{-6}$ K^{-1} and $\alpha_c=9.4(\pm0.1)\times10^{-6}$ K^{-1} for Ti_3SiC_2 and $\alpha_a=8.5(\pm0.1)\times10^{-6}$ K^{-1} and $\alpha_c=9.2(\pm0.1)\times10^{-6}$ K^{-1} for Ti_3GeC_2. A dramatic increase in error bars and a discontinuity in thermal motion parameters of the Ti_{II} atoms in Ti_3GeC_2 were also observed between 300 and 500 °C during both heating and cooling. This discontinuity may in turn explain why the internal friction rises dramatically in that temperature range.

DOI: 10.1103/PhysRevB.82.174109 PACS number(s): 65.40.De, 61.66.Fn, 61.05.fg

I. INTRODUCTION

The ternary compounds Ti_3SiC_2 and Ti_3GeC_2 are members of a class of more than 50 thermodynamically stable nanolaminated solids with the general form $M_{n+1}AX_n$ (*MAX*), where $n=1$, 2, or 3, *M* is an early transition metal, *A* is an *A*-group element, viz., mostly groups 13 and 14, and *X* is either C or N.[1] Since it was discovered that, as a class, the *MAX* phases exhibit unusual yet attractive and sometimes unique combinations of properties, these phases have been studied extensively.[2–5] In addition to having exceptional thermal shock resistance and being excellent electric and thermal conductors, they are elastically quite stiff yet relatively soft and readily machinable, with exceptional damage tolerance.[2,3,6] Some are creep and fatigue resistant.[7–9]

The phases are classified according to their values of *n*, that is "211" for $n=1$, "312" for $n=2$, and "413" for $n=3$. Of particular interest to this work are the 312 *MAX* phases Ti_3SiC_2 and Ti_3GeC_2, which were first synthesized in powder form in the 1960s.[10,11] It was not until recently, however, that they were fabricated and fully characterized in bulk form as fully dense, single-phase solids.[5,6,12] Both phases have a layered hexagonal structure (Fig. 1) belonging to the space group $P6_3/mmc$ (No. 194). Titanium atoms on Wyckoff positions 4*f* (Ti_I, adjacent to the *A* layer) and 2*a* (Ti_{II}, between the C layers) and carbon, C, atoms on Wyckoff position 2*b* result in Ti_3C_2 layers, interleaved with layers of hexagonal nets of pure Si or Ge on Wyckoff position 2*b*.[11] This structure has since been confirmed for Ti_3SiC_2 using convergent beam electron diffraction by Arunajatesan and Carim, who obtained lattice parameters of $a=3.06$ and 17.66 Å.[13]

The chemical bonding and thermal properties of Ti_3SiC_2 have been extensively investigated. Following its discovery and structure verification, a neutron diffraction, ND, study was conducted to confirm the original structure and report bond lengths and bond angles, with lattice parameters $a=3.0575$ Å and $c=17.6235$ Å.[14] In that study, it was found that the Ti-C distances were comparable to normal covalent distances in TiC, whereas the Ti-Si distance was slightly larger than in a normal covalent bond and closer to the sum of metallic Ti and covalent Si radii. Furthermore, a slight distortion of the CTi_6 octahedra, indicated by the distinctly different bond lengths for Ti_I-C and Ti_{II}-C, was noted. Effectively the C atoms relax in the direction of the Si layers (Fig. 1). This results in slightly smaller and more distorted octahedra than in TiC.[14]

Another ND study of Ti_3SiC_2 was conducted soon after in the 298–1273 K temperature range to determine its thermal properties.[15] The coefficients of thermal expansion, CTE, were determined in the *a* and *c* direction to be $8.6(\pm0.1)\times10^{-6}$ K^{-1} and $9.7(\pm0.1)\times10^{-6}$ K^{-1}, respectively, for an average volume expansion of $8.9(\pm0.1)\times10^{-6}$ K^{-1}. The latter is in fairly good agreement with the values determined from dilatometry, viz., $10(\pm1)\times10^{-6}$ K^{-1},[2] 9.2×10^{-6} K^{-1},[5] and $9.1(\pm0.2)\times10^{-6}$ K^{-1}.[15]

Much less information is available for Ti_3GeC_2. A number of papers have been published on $Ti_3Si_xGe_{1-x}C_2$ solid solutions[6,16–19] in which it was shown that both low (4–300 K) temperature transport[18] and mechanical properties[6] are fairly insensitive to *x*. The average of the expansions along the *a* and *c* directions, $8.1(\pm0.2)\times10^{-6}$ K^{-1} and $9.7(\pm0.2)\times10^{-6}$ K^{-1}, respectively, were slightly higher than the dilatometric CTE of Ti_3GeC_2, 7.8×10^{-6} K^{-1}.[20]

While Ti_3GeC_2 and Ti_3SiC_2 are closely related structurally and exhibit similar properties, there are also a number of differences in their thermal and mechanical properties that are not fully understood. For example, the mechanical

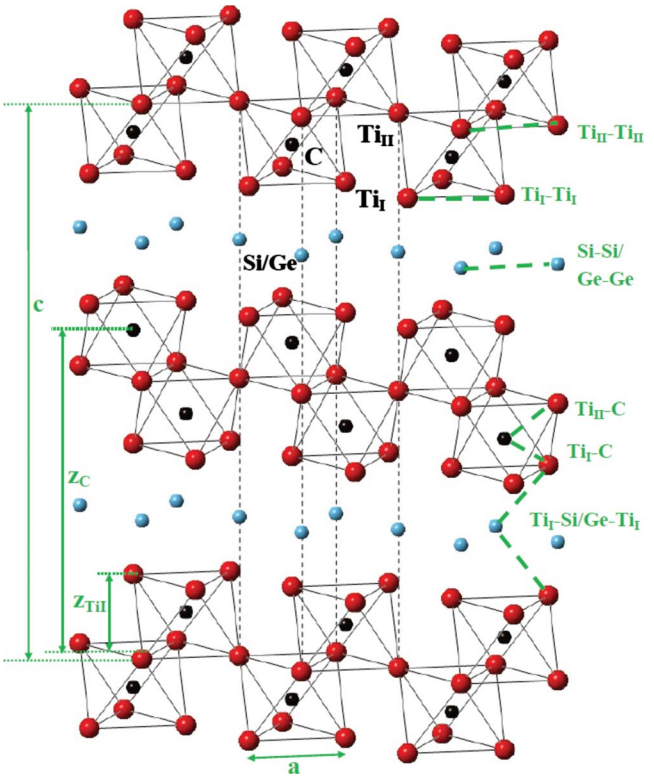

FIG. 1. (Color online) Schematic of Ti_3SiC_2/Ti_3GeC_2 structure, showing lattice parameters a and c, z coordinates of C and Ti_I atoms, positions of Ti_I, Ti_{II}, Ge or Si, and C, and the interatomic distances and angles calculated in this work. Unit cell is delineated by dashed lines.

damping—viz., internal friction, Q^{-1}, determined over the 300–1573 K temperature range—of Ti_3GeC_2, Ti_3SiC_2 and other *MAX* phases was investigated by resonant ultrasound spectroscopy.[21] Up to a critical temperature, Q^{-1} was nearly constant, after which it increased dramatically. This critical temperature was ~1273 K for Ti_3SiC_2 and two other 312 *MAX* phases studied, but only ~623 K for Ti_3GeC_2. Given the otherwise similar properties of Ti_3SiC_2 and Ti_3GeC_2, this was a surprising result. A number of possibilities for explaining this behavior, including increases in the mobility of dislocations and/or other defects such as vacancies in the *A* planes, as well as an order-disorder transition (most probably in the *A* planes), have been postulated.[21] One of the aims of this work is to shed some light on this unexpected mystery by investigating the changes in the crystal structure as a function of temperature.

Herein we use Rietveld analysis of high-temperature ND (HTND) data to study the thermal properties of Ti_3SiC_2 and Ti_3GeC_2 in the 573–1373 K and 373–1273 K temperature ranges, respectively. We report on the lattice parameters, anisotropic displacement factors, bond lengths, and bond angles (and from those the distortion of the coordination polyhedra) as a function of temperature on both heating and cooling. The possibility of dynamic disorder caused by correlated atomic motion at high temperatures for Ti_3GeC_2 and Ti_3SiC_2 is also explored. And while HTND of Ti_3SiC_2 has been carried out previously,[15] we decided to repeat these experiments for three reasons. The first is to enhance the quality of the data. The second is to verify our results and procedures by comparing our data to previous results. The third, and most important reason, is to ensure that the results are comparable to those measured for Ti_3GeC_2 on the same instrument.

II. EXPERIMENTAL DETAILS

A. Sample synthesis

To make the Ti_3GeC_2 sample, a stoichiometric mixture of Ti, C, and Ge powders was ball milled for ~40 min. The powder mixture was then placed in a graphite die and heated in a graphite-heated vacuum hot press, under a mechanical vacuum of 10^{-4} Torr, at a rate of 10 K/min to 1173 K, held for 3 h after which a pressure of ~45 MPa was applied and heating was resumed at the same rate to 1873 K where the sample was held for 6 h before cooling. These samples were subsequently annealed for 48 h in an Ar atmosphere at 1873 K to allow unreacted phases to react and to grow the grains. Further synthesis details can be found elsewhere.[6]

The coarse-grained polycrystalline sample of Ti_3SiC_2 was fabricated by hot isostatic pressing. Ti, SiC, and graphite powders were dry mixed together in a V-blender for 2 h and cold pressed under 180 MPa into bars. The bars were then introduced in a graphite die and hot pressed at 1600 °C under a pressure of ~40 MPa for 4 h to produce coarse-grained microstructure. Further synthesis details can be found elsewhere.[22]

B. Neutron diffraction

HTND experiments were conducted on the high-pressure preferred orientation neutron diffractometer (HIPPO) (Refs. 23 and 24) at the Lujan Neutron Scattering Center, Los Alamos National Laboratory. For both phases, bulk samples were placed in a vanadium holder, mounted in an ILL-type high-temperature vacuum furnace with a vanadium setup (heating elements and heat shields), and heated at a rate of 20 °C/min. Time-of-flight data were collected under vacuum at selected temperature points during heating, and again during cooling, to assess possible hysteresis. Temperature was measured by two type K thermocouples inside the ~15 cm high hot zone of the furnace about 5 cm above the beam center. The data collection temperatures were 300, 500, 700, 900, and 1100 °C for Ti_3SiC_2 and 100, 300, 500, 600, 700, 800, 900, and 1000 °C for Ti_3GeC_2. At each temperature, neutrons were detected with 27 detector panels of ^{3}He detector tubes arranged on three rings with nominal diffraction angles of 40°, 90°, and 144°. The samples were measured at rotation angles of 0°, 45°, 67.5°, and 90° around the vertical axis to allow for a full texture analysis at each temperature. The count time was 15 min per orientation, resulting in 60 min count time per temperature, during which the temperature was held constant for data collection.

C. Structure refinement

The neutron data were analyzed with the Rietveld method using the general structure analysis system (GSAS) (Ref. 25) and material analysis using diffraction/reflectivity (MAUD)

(Ref. 26) software packages. Interference from the adjacent WNR facility was observed in the backscattered 144° bank at time of flight between 15 and 18 ms; this region was excluded from the refinements. Hexagonal structures often exhibit preferred orientation,[27] therefore texture analysis was performed for selected data sets using the E-WIMV (Ref. 28) algorithm as implemented in MAUD. For the GSAS analysis, the data from detectors with the same nominal diffraction angle were integrated and subsequently the four sample orientations were summed up, therefore randomizing preferred orientation effects. A script-controlled multihistogram refinement against the 144°, 90°, and 40° data was performed with GSAS. The crystal structure parameters from the full texture model analyzed with MAUD agreed, within error bars, with the random texture assumed for the GSAS analysis. For both samples, the weak texture observed (see below) was smeared out by integrating the individual detector panels of rings/banks with the same nominal detector angle and then integrating the data of each bank recorded for four different rotations. Therefore the data were analyzed using a script language for GSAS that assumed a random texture. Additional phases were found and refined in both GSAS and MAUD.

The GSAS script-controlled refinement ensures that identical refinement strategies were used on both compositions and the final refinements were conducted with sites fully occupied. For instrument calibration, the room-temperature lattice parameters determined previously from x-ray diffraction (XRD) for Ti_3SiC_2 [a=3.075 Å, c=17.7105 Å (Ref. 22)] and Ti_3GeC_2 [a=3.090 Å, c=17.764 Å (Ref. 6)] were extrapolated to the lowest temperatures, 300 °C and 100 °C, respectively, using the CTE values determined herein. The instrument alignment diffractometer constant parameter, DIFC in GSAS was calibrated to these values for the first runs, i.e., at 300 °C and 100 °C, and fixed for the subsequent runs. Refined parameters were 16 background parameters of GSAS background function no. 1, phase fractions of additional phases, lattice parameters of all phases, atom positions with symmetry constraints (i.e., the z coordinate of the Ti_I and C atoms), instrument calibration (only for the first run), peak width, absorption, and anisotropic thermal motion parameters.

III. RESULTS

A. Texture and composition analysis

Texture analysis of the Ti_3SiC_2 sample [Figs. 2(a)–2(c)] showed very mild texture that did not change with heat treatment. The results of the Ti_3GeC_2 texture analysis [Figs. 2(d)–2(f)] show a mild (0002) fiber texture for the Ti_3GeC_2 phase; again no texture change was observed during heat treatment. As noted above, for both samples, the parameters obtained using MAUD to incorporate preferred orientation were within error bars of those determined by the GSAS with no preferred orientation. Thus the Rietveld analysis described herein was executed in GSAS assuming random texture and full occupancy. Final bond lengths and angles were computed with GSAS.

Table I shows the profile agreement factors for the Rietveld analysis at 300, 500, and 900 °C, giving the weighted pattern R index, wR_p.[29] Figures 3(a) and 3(b) show the Rietveld fit for the neutron time-of-flight data integrated for full detector rings and the four measured orientations for the 90° detector bank at the lowest temperatures for each sample, viz., 300 °C for Ti_3SiC_2 [Fig. 3(a)] and 100 °C for Ti_3GeC_2

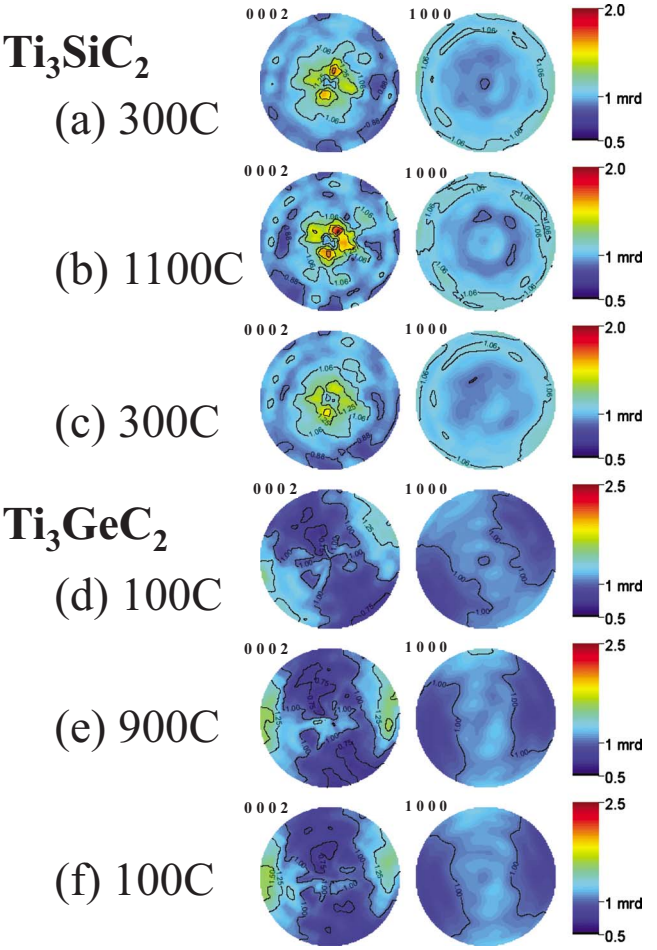

FIG. 2. (Color online) Pole 0002 and 1000 figures recalculated from the orientation distribution of HIPPO data for (a) Ti_3SiC_2 at 300 °C (before heating), (b) 1100 °C, (c) 300 °C (after heating) and, (d) Ti_3GeC_2 at 100 °C (before heating), (e) 900 °C and, (f) 100 °C (after heating).

TABLE I. Profile agreement factors for Rietveld refinements for neutron-diffraction data collected during heating and cooling.

Temperature (°C)	wR_p (%)	
	Ti_3SiC_2	Ti_3GeC_2
300	1.84	1.88
500	1.60	2.00
900	1.49	2.45
900[a]	1.51	2.40
500[a]	1.63	2.23
300[a]	1.69	2.12

[a]Data collected during cooling.

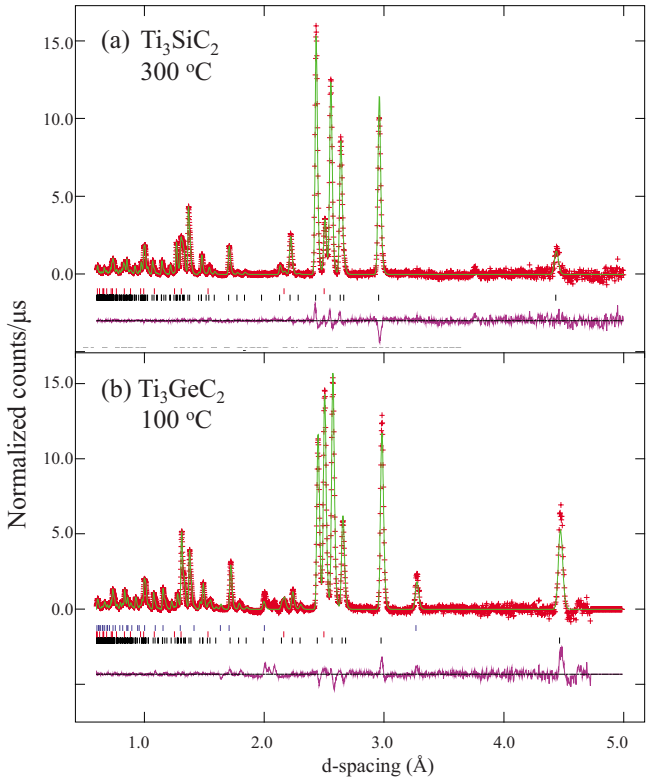

FIG. 3. (Color online) Rietveld refinement of HIPPO data from 90° detector bank for (a) Ti_3SiC_2 at 300 °C and, (b) Ti_3GeC_2 at 100 °C. In both plots, the raw data points are shown as red + and the calculated profile is shown as a solid green line. Underneath, markers show calculated peak positions for each phase. From top to bottom: pure Ge in blue (Ti_3GeC_2 only), TiC in red, and Ti_3GeC_2/Ti_3SiC_2 in black. Difference curve ($y_{obs}-y_{calc}$) is shown as a solid purple line below.

[Fig. 3(b)]. The calculated (solid lines) and observed (+ signs) data are compared. Below these, from top to bottom, are the markers showing peak positions for the included phases Ge [Fig. 3(b) only], TiC, and Ti_3SiC_2 or Ti_3GeC_2, and the difference curves, $y_{obs}-y_{calc}$.

In both phases, TiC, with a rocksalt structure (space group $Fm\bar{3}m$),[30] was an impurity phase. The TiC content was 5.8(±0.2) wt % in Ti_3SiC_2 and 19.1(±0.3) wt % in Ti_3GeC_2. These fractions remained constant with thermal cycling. Peaks corresponding to 3.0(±0.3) wt % Ge—with a cubic structure (space group $Fm\bar{3}m$)—in the Ti_3GeC_2 sample were also found. At temperatures above 900 °C, the Ge peaks disappeared, in agreement with its melting point at 917 °C.[31] At temperatures 900 °C and lower, the fraction of Ge also remained constant upon thermal cycling. No other reactions or phase changes were observed during the thermal cycling. In the Ti_3GeC_2 sample, another minor impurity phase—with diffraction peaks near 1.8 and 2.1 Å—could not be identified. Peaks above ~2.12 Å from this phase were not observed, and based on the relative peak intensities and their positions we assume it is a cubic, trigonal, or hexagonal structure with a relatively small unit cell. Since the inclusion, or exclusion, of less than 4 wt % Ge in the refinements had very little, if any, effect on the refined Ti_3GeC_2 structural parameters, we assume that our refined parameters for Ti_3GeC_2 are also not affected by this unaccounted impurity phase.

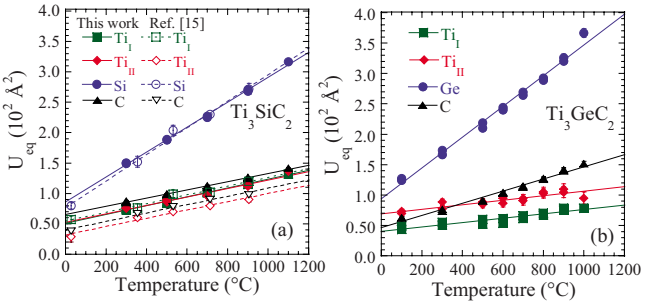

FIG. 4. (Color online) Temperature dependence of equivalent isotropic thermal motion U_{eq} during heating and cooling for atoms in, (a) Ti_3SiC_2 measured herein and those taken from Ref. 15 and, (b) Ti_3GeC_2 (this work).

B. Atomic displacement

In structure refinement, the Debye-Waller factor (T) that accounts for the thermal motion correction to the structure factor due to anisotropic thermal motion is expressed as

$$T = \exp[-2\pi^2(U_{11}h^2a^{*2} + U_{22}k^2b^{*2} + U_{33}l^2c^{*2} + 2U_{23}klb^*c^* + 2U_{13}lhc^*a^* + 2U_{12}hka^*b^*)], \quad (1)$$

where a^*, b^*, and c^* are the edges of the unit cell in reciprocal space associated with the x^*, y^*, and z^* axes, respectively.[25] For hexagonal structures, due to site symmetry U_{23} and U_{13} are both equal to 0 and the equation simplifies:

$$T = \exp[-2\pi^2(U_{11}h^2a^{*2} + U_{22}k^2b^{*2} + U_{33}l^2c^{*2} + 2U_{12}hka^*b^*)]. \quad (2)$$

For the hexagonal crystal system, these anisotropic U_{ij}'s may be converted to an approximated isotropic temperature factor U_{eq} given by

$$U_{eq} = 1/3(U_{11} + U_{22} + U_{33} - U_{12}). \quad (3)$$

Figures 4(a) and 4(b) plot the temperature dependencies of U_{eq} for the four unique atoms in Ti_3SiC_2 and Ti_3GeC_2, respectively. The standard deviations were calculated as outlined by Schomaker and Marsh.[32] Also plotted in Fig. 4(a) are previous results obtained on Ti_3SiC_2.[15] The agreement between the two sets of results is excellent, lending validity to both. The U_{eq}'s of all atoms increase approximately linearly with temperature, with the greatest increases in U_{eq}'s occurring for the A-group atoms in both materials. At all temperatures, the U_{eq}'s for Ge are higher than those of Si. Note that in most plots, both heating and cooling results are displayed. In all but one case, Ti_{II} in Ti_3GeC_2(see below), the agreement between both is excellent. In figures where the error bars are not included, it follows they were smaller than the symbols used.

The temperature dependencies of the U_{ij}'s for the four unique atoms in Ti_3SiC_2 (shown in red) and Ti_3GeC_2 (shown

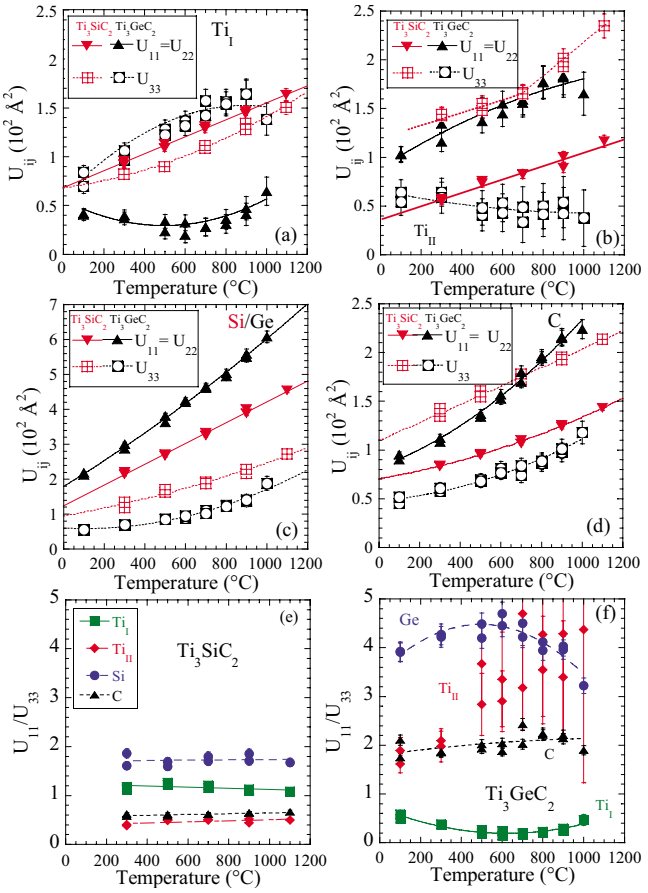

FIG. 5. (Color online) Temperature dependence of anisotropic U_{ij}'s in Ti_3SiC_2 (red) and Ti_3GeC_2 (black) during heating and cooling for, (a) Ti_I, (b) Ti_{II}, (c) Si/Ge, and (d) C. The U_{11}/U_{33} ratios for the various atoms in, (e) Ti_3SiC_2 and, (f) Ti_3GeC_2 during heating and cooling.

in black) are compared in Figs. 5(a)–5(d). The results for the Si/Ge atoms are more comparable [Fig. 5(c)] but here again the Ge atoms vibrate more vigorously and anisotropically than the Si atoms. Surprisingly, the U_{ij}'s of Ti_I, Ti_{II}, and C are quite different, not only in magnitude, but more importantly in their temperature dependencies and relative values. To better appreciate these differences, the temperature dependencies of the ratios of thermal motions in the a and c directions, viz., U_{11}/U_{33}, are plotted for Ti_3SiC_2 and Ti_3GeC_2 in Figs. 5(e) and 5(f), respectively. And while both the Si and Ge atoms tend to vibrate more along the basal planes than along the c axis (i.e., $U_{11}/U_{33}>1$), the extent of this anisotropic motion is much greater for Ge, with U_{11}/U_{33} values that are more than twice those of Si [compare Figs. 5(e) and 5(f)]. Note that the error bars associated with Ti_{II} atoms in Ti_3GeC_2 suddenly increase dramatically between 300 and 500 °C [Fig. 5(f)]. This is not an experimental artifact, however, since, (i) the error bars for the same atoms in Ti_3SiC_2 are quite low [Fig. 5(e)] and, (ii) the error bars at 100 and 300 °C for Ti_3GeC_2 are also quite low.

To further accentuate the differences, the thermal ellipsoids at three different temperatures are compared in Figs. 6 and 7 for Ti_3SiC_2 and Ti_3GeC_2, respectively. A major difference between the two structures is the extent to which the Ge

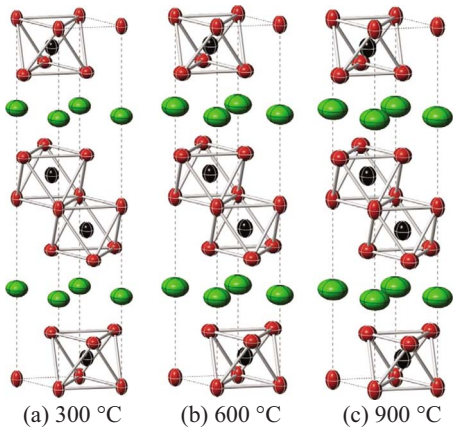

FIG. 6. (Color online) Thermal ellipsoids (99% probability) of Ti (red), Si (green), and C (black) in Ti_3SiC_2 at (a) 300 °C, (b) 600 °C, and (c) 900 °C. Images generated using CRYSTALMAKER (Ref. 33).

ellipsoids are flattened relative to those of Si. Note that the Ti_{II} atoms in Ti_3GeC_2 also flatten along the basal planes with increasing temperature. The Ti_I atoms, on the other hand, tend to vibrate normal to the basal planes.

C. Atomic distances, thermal expansion, and bond angles

The strains along the a and c axes are also plotted in Figs. 8(b) and 8(c), and their values are listed in Table II along with the unit cell volumes. Least-squares fits of the lattice parameters and unit cell volumes yield thermal-expansion coefficients of $8.9(\pm0.1)\times10^{-6}$, $9.4(\pm0.1)\times10^{-6}$, and $9.0(\pm0.1)\times10^{-6}$ K^{-1} for Ti_3SiC_2 in the a direction, c direction, and the volume expansion, respectively. For Ti_3GeC_2, the respective CTE values are $8.5(\pm0.1)\times10^{-6}$, $9.2(\pm0.1)\times10^{-6}$, and $8.7(\pm0.1)\times10^{-6}$ K^{-1}.

The only atom positions that are unconstrained by the $P6_3/mmc$, (No. 194) space group are the z coordinates of the Ti_I and C atoms, which are listed in Table III for both Ti_3SiC_2 and Ti_3GeC_2. The interatomic distances at each tem-

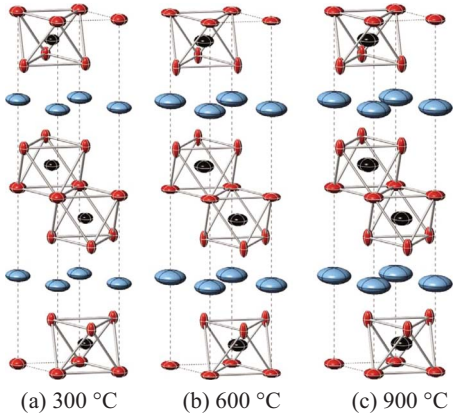

FIG. 7. (Color online) Thermal ellipsoids (99% probability) of Ti (red), Ge (blue), and C (black) in Ti_3GeC_2 at (a) 300 °C, (b) 600 °C, and, (c) 900 °C. Images generated using CRYSTALMAKER (Ref. 33).

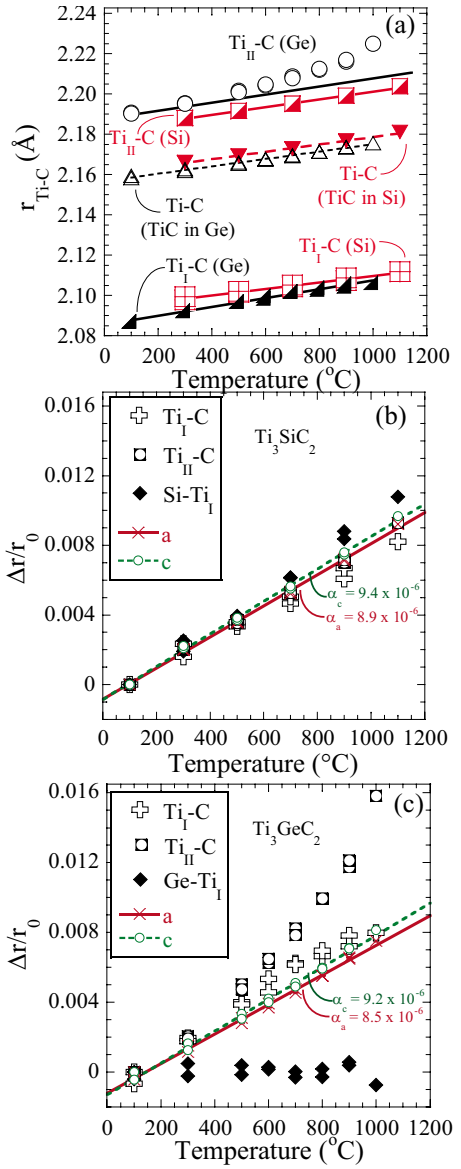

FIG. 8. (Color online) (a) Atomic distances between the Ti and C in Ti_3SiC_2 (red), Ti_3GeC_2 (black), and TiC during heating and cooling. For lines labeled TiC, the red and black markers correspond to this impurity phase in the Ti_3SiC_2 and Ti_3GeC_2 samples, respectively. (b) and (c) show the temperature dependencies of the thermal strains of the lattice parameters and interatomic distances in Ti_3SiC_2 and Ti_3GeC_2, respectively. For Ti_3SiC_2, the 100 °C values were extrapolated and used for r_0 for comparison's sake.

perature during heating and cooling, as well as room temperature values determined in previous work,[14–16,34,35] are listed in Table IV. Based on these results, the order of the Ti-C bonds lengths, in increasing order, is Ti_{II}-C(Ti_3GeC_2) $\approx$ Ti_{II}-C(Ti_3SiC_2) < Ti_I-C(Ti_3SiC_2) < Ti_I-C(Ti_3GeC_2) [see Table IV, Fig. 8(a)]. Also plotted for comparison in Fig. 8(a) are the Ti-C distances in the TiC secondary phases present in the samples. For both ternary structures, the Ti_I-C bonds are shorter than, while the Ti_{II}-C bonds are longer than, the Ti-C distance in TiC. However, the Ti_{II}-C distance in Ti_3GeC_2 not only is longer than that in Ti_3SiC_2 but shows the only clearly nonlinear increase with temperature of all bonds [Figs. 8(a) and 8(c)]. This nonlinear increase is indicated by an increase in the C-atom z coordinate, z_C (Table III). The z coordinate for C in Ti_3SiC_2, on the other hand, stays constant with temperature, as expected for a structure whose bond lengths expand at the same rate as the lattice parameters. All other Ti-C bonds increase at a rate similar to that in TiC [Fig. 8(a)].

The interatomic distances in Ti_3SiC_2 increase more or less linearly with temperature, with the Si-Ti bond distances increasing slightly more than the bonds in the Ti-C octahedra (Table IV). This is also clear in Fig. 8(b) where the thermal expansions of each bond are plotted for Ti_3SiC_2. The thermal strains in Ti_3GeC_2, however, are markedly different [Fig. 8(c)]. In this case the Ti_{II}-C bonds increase dramatically and nonlinearly, starting roughly at 500 °C, while the Ti_I-Ge bonds appear *not* to increase in length at all with temperature [Fig. 8(c)].

The temperature dependencies of the bond angles—labeled in Fig. 1—in Ti_3SiC_2 and Ti_3GeC_2 are shown in Fig. 9. The Ti_I-Si/Ge-Ti_I bond angles (shown in top half in Fig. 9) represent the displacement of the Ti_I layers either in the direction of, or away from, the Si/Ge layers. The C-Ti_{II}-C angles (shown in the middle of Fig. 9) represent the compression, or expansion, around the Ti_{II} atoms shared by CTi_6 octahedra above and below the Ti mirror plane. The Ti_I-C-Ti_{II} angles (shown in the bottom half of Fig. 9) represent the distortion of the Ti-C layers. From these results it is obvious that for Ti_3GeC_2, the Ti_I-Ge-Ti_I bond angles decrease with increasing temperature; the corresponding Ti_I-Si-Ti_I angles for Ti_3SiC_2 increase slightly. Conversely, the Ti_I-C-Ti_{II} and C-Ti_{II}-C bond angles for Ti_3GeC_2 increase slightly with increasing temperatures; those for Ti_3SiC_2 are more or less independent of temperature as in cubic TiC.

IV. DISCUSSION

The most surprising result of this work, and the leitmotiv of this discussion, is the striking differences in the *anisotropic* thermal motion properties between Ti_3SiC_2 and Ti_3GeC_2 [Figs. 5(e) and 5(f); Fig. 6; Fig. 7]. Even more intriguingly, the same is *not* true of the equivalent *isotropic* thermal motion parameters [Figs. 4(a) and 4(b)] and the thermal expansions along the a and c axes [Figs. 8(b) and 8(c)]. Before addressing possible reasons for this state of affairs and their implications, it is important to discuss the results obtained in light of what is known about the thermal properties of Ti_3SiC_2, Ti_3GeC_2 and TiC.

The results presented herein are consistent with what is currently known about Ti_3SiC_2. This is best seen in Fig. 4(a) where the results from Ref. 15 are superimposed on those measured herein. We note in passing that the quality of the results obtained herein is superior, with significantly less noise. We also note that in all figures the error bars are either smaller than the width of the symbols used or are shown.

For Ti_3GeC_2 there are no ND data to compare our results with. The only benchmark for the anisotropic atomic displacement parameters we are aware of are the room-temperature single-crystal x-ray results for the solid solution, $Ti_3Si_{0.43}Ge_{0.57}C_2$, reported by Yang *et al.*[36] (Note that Ti_1 and Ti_{II} are swapped herein.) In agreement with the single-crystal

TABLE II. Summary of lattice parameters and unit-cell volumes obtained from Rietveld refinements of HTND data (numbers in parentheses are estimated standard deviations in the last significant figure of the refined parameter), and room temperature values reported in Refs. 15, 16, and 34.

	Ti_3SiC_2			Ti_3GeC_2		
T (°C)	a (Å)	c (Å)	V (Å^3)	a (Å)	c (Å)	V (Å^3)
RT (Ref. 16)	3.0665	17.671	143.906	3.0874	17.806	146.990
RT (Ref. 15)	3.06557(6)	17.6300(5)	143.485(9)			
RT (Ref. 34)[a]	3.0705	17.670	144.273	3.0823	17.711	145.721
100				3.08793(5)	17.8193(5)	147.149(4)
300	3.07468(3)	17.7190(3)	145.067(2)	3.09259(5)	17.8484(5)	147.833(4)
500	3.07947(3)	17.7477(3)	145.756(2)	3.09752(6)	17.8786(5)	148.557(5)
600				3.10003(6)	17.8943(6)	148.928(6)
700	3.08465(3)	17.7798(3)	146.510(2)	3.10259(7)	17.9103(7)	149.308(6)
800				3.10497(7)	17.9258(7)	149.666(6)
900	3.09045(3)	17.8144(3)	147.348(3)	3.10822(8)	17.9456(7)	150.145(7)
1000				3.11111(9)	17.9644(8)	150.582(8)
1100	3.09687(3)	17.8532(3)	148.284(3)			
900[b]	3.09078(3)	17.8166(3)	147.398(3)	3.10800(8)	17.9453(8)	150.121(7)
800[b]				3.10491(7)	17.9246(7)	149.650(6)
700[b]	3.08507(3)	17.7822(3)	146.570(3)	3.10196(7)	17.9065(6)	149.215(6)
600[b]				3.09928(6)	17.8902(6)	148.822(5)
500[b]	3.07972(3)	17.7500(3)	145.797(2)	3.09654(6)	17.8735(6)	148.420(5)
300[b]	3.07484(3)	17.7212(3)	145.101(2)	3.09149(5)	17.8416(5)	147.672(5)
100[b]				3.08655(5)	17.8115(5)	146.953(4)

[a]Based on first-principles calculations.
[b]Data collected during cooling.

data, we find a strong anisotropy for the A atoms. Our U_{11} and U_{22} values are about twice as large when extrapolated to RT as those of Yang *et al.* Similarly, our anisotropic thermal motion parameters extrapolated to RT for Ti and C atoms are consistently higher by about a factor of 2 relative to the single crystal results for the solid-solution sample and exhibit substantial anisotropy. These differences can be attributed to the differences in compositions.

Our bond lengths for both compounds are also consistent with those estimated at room temperature from XRD results by Gamarnik and Barsoum[16] (see Table IV). Furthermore, the expansions along the a and c directions measured herein—$8.5(\pm 0.1)\times 10^{-6}$ K^{-1} and $9.2(\pm 0.1)\times 10^{-6}$ K^{-1}—are in good agreement with those measured by high-temperature XRD, viz., $8.1(\pm 0.2)\times 10^{-6}$ K^{-1} and $9.7(\pm 0.2)\times 10^{-6}$ K^{-1}, respectively.[20] Again, the quality of the results obtained here are superior to those measured previously[18,20] and are the ones that should be adopted.

From the results shown in Fig. 8(a), we estimate the CTE of the impurity TiC phase, in both Ti_3SiC_2 and Ti_3GeC_2 to be $8.5(\pm 0.1)\times 10^{-6}$ K^{-1}. These values are higher than the 7.0×10^{-6} K^{-1} (Ref. 30) or 7.4×10^{-6} K^{-1} (Ref. 37) reported for near-stoichiometric TiC in previous studies. The reason for this state of affairs is not totally clear at this time, but could be due to either the fact that the TiC in the ternaries is nonstoichiometric and/or the result of thermal residual stresses. The measured TiC lattice parameters suggest it was stoichiometric.

The bulk CTE of composites–as measured with a dilatometer–follow, to a good approximation, the rule for mixtures whereas the phase specific CTEs measured by diffraction techniques adapt to the constraints imposed by the

TABLE III. z coordinates of Ti_I and C atoms in Ti_3SiC_2 and Ti_3GeC_2 obtained from Rietveld refinements of HTND data. Numbers in parentheses are estimated standard deviations in the last significant figure of the refined parameter.

	Ti_3SiC_2		Ti_3GeC_2	
T (°C)	z_{TiI}	z_C	z_{TiI}	z_C
100			0.13245(9)	0.57148(4)
300	0.13529(5)	0.57218(3)	0.1327(1)	0.57161(5)
500	0.13532(5)	0.57218(3)	0.1330(1)	0.57187(6)
600			0.1332(1)	0.57196(7)
700	0.13523(5)	0.57218(3)	0.1334(1)	0.57219(8)
800			0.1335(1)	0.57238(8)
900	0.13509(6)	0.57214(3)	0.1337(1)	0.5725(1)
1000			0.1342(1)	0.5732(1)
1100	0.13512(7)	0.57217(4)		

TABLE IV. Selected interatomic distances (Å) deduced from Rietveld refinements of HTND data, and room-temperature values reported in Refs. 10, 14–16, and 34. Interatomic distances in secondary phase TiC also included for comparison. Numbers in parentheses are estimated standard deviations in the last significant figure of the refined parameter.

T	Ti_3SiC_2				Ti_3GeC_2				TiC	
(°C)	Si-Ti_I	Ti_I-Ti_I	Ti_I-C	Ti_{II}-C	Ge-Ti_I	Ti_I-Ti_I [a]	Ti_I-C	Ti_{II}-C	Ti–C[b]	Ti–C[c]
RT (Ref. 10)	2.696	3.068	2.135[d]							
RT (Ref. 14)	2.681	3.0575	2.088	2.176						
RT (Ref. 15)	2.693(2)	3.06557(6)	2.085(2)	2.1814(8)						
RT (Ref. 16)	2.6263	3.0665	2.1609[d]		2.6754	3.0874	2.1646[d]			
RT (Ref. 34)[e]	2.6697	3.0705	2.0931	2.2033	2.6898	3.0823	2.0943	2.2078		
100					2.7521(14)	3.08793(5)	2.0871(11)	2.1907(5)		2.15939(3)
300	2.6987(7)	3.07468(3)	2.0978(6)	2.18798(28)	2.7516(15)	3.09259(5)	2.0924(12)	2.1954(5)	2.16623(7)	2.16267(3)
500	2.7025(7)	3.07947(3)	2.1015(6)	2.19140(28)	2.7512(17)	3.09752(6)	2.0968(14)	2.2016(6)	2.16943(7)	2.16612(4)
600					2.7506(19)	3.10003(6)	2.0999(16)	2.2043(7)		2.16788(4)
700	2.7084(7)	3.08465(3)	2.1043(6)	2.19516(30)	2.7493(21)	3.10259(7)	2.1020(18)	2.2086(8)	2.17293(7)	2.16968(5)
800					2.7503(22)	3.10497(7)	2.1030(19)	2.2121(9)		2.17136(5)
900	2.7156(8)	3.09045(3)	2.1073(7)	2.19893(34)	2.7507(25)	3.10822(8)	2.1057(21)	2.2159(10)	2.17679(7)	2.17359(5)
1000					2.7470(29)	3.11111(9)	2.1062(25)	2.2248(12)		2.17566(6)
1100	2.7209(10)	3.09687(3)	2.1118(8)	2.2039(4)					2.18105(8)	
900[f]	2.7144(8)	3.09078(3)	2.1086(7)	2.1992(4)	2.7507(26)	3.10800(8)	2.1044(22)	2.2170(11)	2.17693(8)	2.17347(6)
800[f]					2.7485(22)	3.10491(7)	2.1037(19)	2.2124(9)		2.17126(5)
700[f]	2.7085(7)	3.08507(3)	2.1052(6)	2.19510(32)	2.7490(20)	3.10196(7)	2.1018(17)	2.2077(8)	2.17300(7)	2.16914(5)
600[f]					2.7502(19)	3.09928(6)	2.0984(16)	2.2047(7)		2.16729(4)
500[f]	2.7023(7)	3.07972(3)	2.1020(6)	2.19170(29)	2.7495(18)	3.09654(6)	2.0968(14)	2.2009(7)	2.16937(7)	2.16537(4)
300[f]	2.6971(6)	3.07484(3)	2.0994(5)	2.18804(26)	2.7492(16)	3.09149(5)	2.0922(13)	2.1951(6)	2.16611(7)	2.16178(4)
100[f]					2.7489(14)	3.08655(5)	2.0870(11)	2.1903(5)		2.15837(3)

[a]Due to symmetry, $r_{Ge\text{-}Ge}=r_{Ti1\text{-}Ti1}=r_{Ti2\text{-}Ti2}=a$.
[b]TiC in Ti_3SiC_2 sample.
[c]TiC in Ti_3GeC_2 sample.
[d]$r_{Ti1\text{-}C\text{-}Ti2}/2$.
[e]Based on first principles calculations.
[f]Data collected during cooling.

composite and will thereby be different from the values for the pure phases. In our case, the higher CTE values observed for TiC compared to reported values for pure TiC are consistent with the constraint imposed by the more rapid shrinkage of the *MAX* phases from high temperatures. Similarly, the CTE values reported for the *MAX* phases are to be considered lower bounds, since their values for phase pure samples would be higher. (Ge also has a lower CTE than Ti_3GeC_2).

The fact that the CTEs of TiC_x are within error bars identical $[8.5(\pm 0.1)\times 10^{-6}]$ in both compounds, despite the fact that the TiC_x content in the Ti_3GeC_2 sample was $\approx$4 times that in Ti_3SiC_2, is taken as strong evidence that any stresses caused by differences in CTE do not play a significant role. This comment notwithstanding, it is hereby acknowledged that why the CTE of the TiC phase is as high as it is, especially if it is stoichiometric, is not clear. It should also be noted that the Ge and TiC_x phase fractions remain constant during heating (with the exception of the melting of Ge between 900 and 1000 °C), implying that no reactions take place as a result of heating.

One of the hallmarks of the *MAX* phases comprised of elements with atomic numbers higher than Al is that the *A*-group elements act as "rattlers"—i.e., atoms that vibrate significantly more than other atoms—in the structure.[1] It is this rattling effect that is believed to be responsible for the low phonon conductivities of the *MAX* phases comprised of elements heavier than Al, despite their high specific stiffness values and high Debye temperatures.[1,18,19] The results shown in Figs. 4(a) and 4(b) not only confirm this notion for Ti_3GeC_2 (compare the full scales of the *y* axes for Si/Ge and the other atoms in Fig. 5) but as important show that Ge is even more of a rattler than Si [Fig. 5(c)]. The latter conclusion is in accordance with the fact that the phonon conductivity of Ti_3GeC_2 at room temperature is negligible[1,18] despite having a Young's modulus of over 340 GPa.[18,21]

We now turn to the most surprising result of this work, viz., the apparent lack of expansion of the Ti_I-Ge bonds compared to the more normal response of the Ti_I-Si bonds [Figs. 8(b) and 8(c)]. This is derived from the increase in the *z* coordinate (Table III) for the Ti_I atom with temperature (see Fig. 1). Note that in Ti_3SiC_2, the *z* coordinates for both Ti_I and C remain constant with temperature since all interatomic distances essentially increase uniformly with temperature. The most likely explanation for the discrepancies can be re-

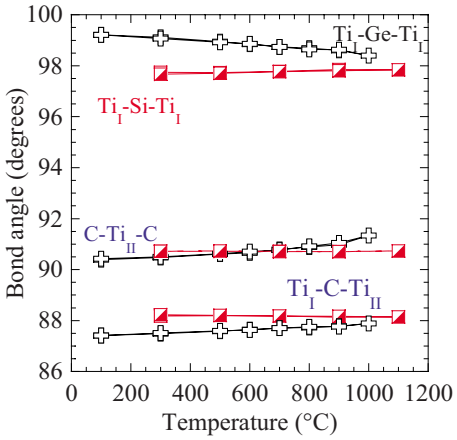

FIG. 9. (Color online) Bond angles in Ti_3SiC_2 (red squares) and Ti_3GeC_2 (black crosses) between atoms in Ti layers with *A*-group (Si or Ge) layers (top) and C layers (middle and bottom).

lated to the pronounced anisotropic motion of the Ge atoms, together with the resulting correlated motions of the Ti_I and Ge atoms. More specifically, the orbiting motion of the *A* atoms around their average position in the *a*-*b* plane was proposed by Togo *et al.*,[38] who showed, using first-principles phonon calculations, that essentially the Ti_I and Ge atoms avoid each other as much as possible. Our argument (and evidence) is as follows: (i) The repulsion of the Ti_I atom is reduced temporarily when the Ge atom is displaced in the basal plane away from that Ti_I atom [see r_2 in Fig. 10(a)], and the Ti_I atoms can move closer to the Ge plane. (ii) This in turn is evidenced by the fact that the Ti_I atoms vibrate more normal to the basal planes than parallel to them. (iii) If the Ti_I and Ge atomic motions are correlated, then the instantaneous bond lengths may be approximated by the distances r_1 and r_2 [Fig. 10(a)] between the edges of the 50% probability thermal ellipsoids. [Note that 99% probability ellipsoids are used in Fig. 10(a) to emphasize the effect.] In Fig. 10(b), r_1 and r_2 are plotted as triangles and circles, respectively. The average of these two numbers is given by the red squares [Fig. 10(b)]. Also shown on the same figure are the values directly obtained from Rietveld analysis, i.e., distance r_3 in Fig. 10(a), and denoted as blue crosses in Fig. 10(b). In light of these calculations, the result that r_3 does not increase with temperature is but a consequence of the *anisotropic* and *correlated* motions of the Ge atoms in the basal planes. A similar effect was reported by Tucker *et al.* in quartz, explained by the difference between the instantaneous and average positions of Si and O atoms.[39]

The Si thermal ellipsoids, on the other hand, show thermal motion that is less anisotropic (Fig. 6). Since the Si thermal ellipsoids are not as flattened as those of Ge, the Ti_I atom does not vibrate preferentially normal to the plane into the space provided, as it does in Ti_3GeC_2. Consequently, in Ti_3SiC_2, the Ti_I atoms vibrate with slight preference in the basal planes, whereas the Ti_I atoms in Ti_3GeC_2 vibrate anisotropically normal to the basal planes. A possible reason for the difference in the thermal behavior of the Si and Ge atoms is their atomic masses relative to the Ti atoms. Since Si is lighter than Ti, it is not unreasonable to conclude that their correlated motion is not as strong and thus less anisotropic. Conversely, because the Ge atom is heavier than Ti, the correlated motion effect is stronger. Consistent with these notions is the fact that the Al in Ti_4AlN_3 (Ref. 40) behaves more like Si in Ti_3SiC_2.

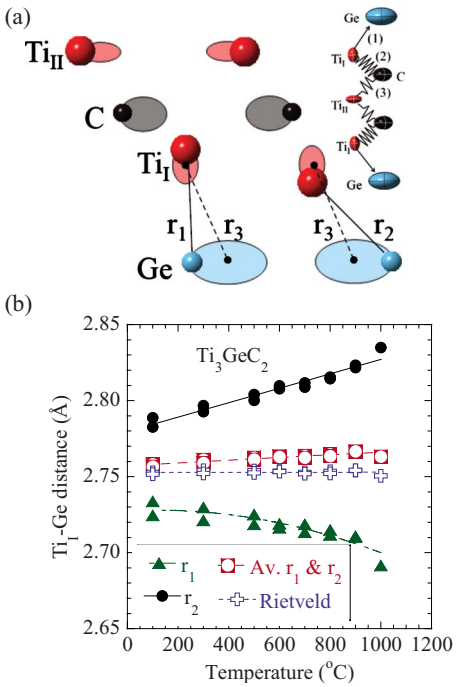

FIG. 10. (Color online) Schematic of, and interatomic distances in Ti_3GeC_2, (a) 99% probability thermal ellipsoids at 1000 °C showing Ti_I-Ge instantaneous positions (solid lines, r_1 and r_2) and interatomic distance between time-averaged positions (dashed lines, r_3). Inset, top right, sketches the interatomic distance behavior with (1) the movement of Ti_I toward the empty space provided by the Ge thermal motion, (2) the more rigid bond between Ti_I and C, and (3) the relatively weaker bond between Ti_{II} and C. (b) Temperature dependence of the Ti_I-Ge bond showing the minimum (r_1, green triangles) and maximum (r_2, black circles) interatomic distances for the 50% probability thermal ellipsoids, the average of the two (red squares), and the distances determined by the time- and space-averaged positions obtained by Rietveld analysis (blue crosses).

Based on the shape of the Ti_I thermal ellipsoids in Ti_3SiC_2, it is reasonable to assume that the correlated motion of the Ti_I is in the basal plane rather than normal to it. The instantaneous positions can therefore be approximated by distances r_4 and r_5 [Fig. 11(a)]. Here the distance determined by Rietveld analysis is given by r_6 [Fig. 11(a)]. In this case, the average of the two "instantaneous" positions, plotted as red squares in Fig. 11(b), are almost identical to the values obtained from the Rietveld refinement shown as blue crosses in Fig. 11(b). The end result is, again, quite reasonable, but because the Si motion is less anisotropic, the increase in the Ti_I-Si bond behaves more "normally"—it expands with temperature. It is important to note that when the results shown in Figs. 10(b) and 11(b) are superimposed, at 1.71×10^{-5} K^{-1} the thermal expansion of r_2 is only ≈20% smaller than that of r_5 at 2.17×10^{-5} K^{-1}. Said otherwise, the expansions are not as different as the ratio of the expansions, derived simply from Rietveld analysis, viz. r_3/r_6

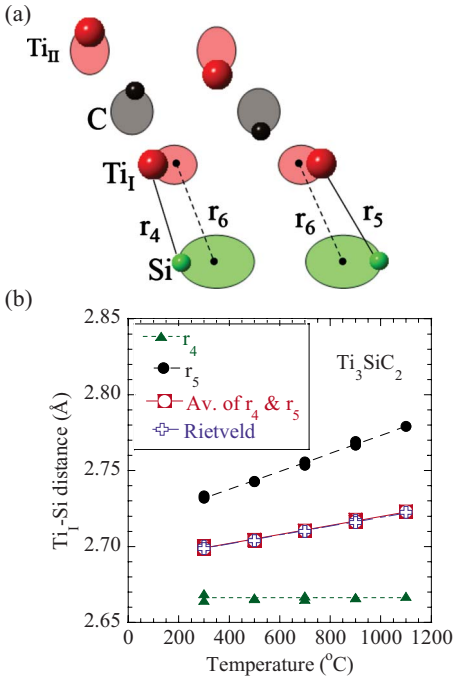

FIG. 11. (Color online) Schematic of, and interatomic distances in, Ti_3SiC_2: (a) 99% probability thermal ellipsoids 1100 °C showing Ti_I-Si instantaneous positions (solid lines, r_4 and r_5) and interatomic distance between time-averaged positions (dashed lines, r_6). (b) Temperature dependence of the Ti_I-Si bond showing the minimum (r_4, green triangles) and maximum (r_5, black circles) interatomic distances for the 50% probability thermal ellipsoids, the average of the two (red squares), and the distances determined by the time- and space-averaged positions obtained by Rietveld analysis (blue crosses).

≈0.002, would suggest. For comparison's sake the thermal expansion of the Ti_{II}-C bond [Fig. 8(c)] is $\approx 1.6\times10^{-5}$ K^{-1}. Thus, in the final analysis, the expansion of the Ti_I-Si and Ti_I-Ge bonds are comparable to those of the Ti_{II}-C bonds.

The anisotropic vibrations of the Ge atoms are also manifested in the bond angles. In the case of Ti_3SiC_2, the lattice expands more or less uniformly and the angles (Fig. 9) are weak functions of temperature. In contrast, in Ti_3GeC_2 the expansion is accompanied by a decrease in the Ti_I-Ge-Ti_I angle with a concomitant and almost equal increase in the C-Ti_{II}-C angle. This observation is most easily explained as follows: since the Ti_I-C bond is significantly shorter than the Ti_{II}-C bond and therefore presumably stronger [Fig. 8(a)], the C atom follows the temporary displacement of the Ti_I atom toward the *A* plane as the Ge atoms move away as discussed above. But since the Ti_{II} atoms are located on a mirror plane, they cannot accommodate the Ti_I displacement toward the *A* plane and the Ti_{II}-C bond thus expands at a higher rate than the Ti_I-C bond [see sketch in inset of Fig. 10(a)]. Said otherwise, the C-Ti_{II}-C and Ti_I-Ge-Ti_I bond assemblies, being the weakest, act as hinges that move in opposite directions.

In both compounds, the Ti_I-C bonds are almost identical [Fig. 8(a)]. And while shorter than the Ti-C bonds in TiC, their rates of expansion are very similar to the latter [Fig. 8(a)]. In contradistinction, the response of the Ti_{II}-C bonds in Ti_3GeC_2 is not "normal" [Fig. 8(a)] for the reasons outlined above.

Lastly, we address how this unique understanding sheds light on why the internal friction in Ti_3GeC_2 increases dramatically at ≈427 °C. A perusal of the results presented herein indicate that a discontinuity of sorts occurs between 300 and 500 °C in Ti_3GeC_2. This is best seen in Figs. 8(a) and 8(c) where it is clear that a large increase in the Ti_{II}-C bond lengths occurs between 300 and 500 °C. Another hint, which may be more relevant, can be found in Fig. 5(f). Below 400 °C, the error bars and the scatter in the anisotropies of vibration of the Ti_{II} atoms are quite low, reproducible and consistent with the results for the Ti_{II} atoms in Ti_3SiC_2; above that temperature, however, the noise level increases dramatically, not only at a given temperature, but between heating and cooling. Such noise is unique to the Ti_{II} atoms in Ti_3GeC_2. At this time we cannot explain the discontinuity observed between 300 and 500 °C in the U_{11}/U_{33} ratio for the Ti_{II} atoms [Fig. 5(f)] or the increase in noise level. We speculate that the dramatic increase in uncertainty is an indication that the thermal motion of Ti_{II} cannot be described by an ellipsoid at temperatures above 300–500 °C. High-resolution high-temperature neutron powder-diffraction data that will be analyzed by pair-distribution function and entropy mechanisms, of both Ti_3SiC_2 and Ti_3GeC_2, will be collected in the near future to experimentally verify this hypothesis.

V. SUMMARY AND CONCLUSIONS

Herein we report on the thermal properties of Ti_3SiC_2 and Ti_3GeC_2 as deduced from Rietveld analysis of HTND data. At all temperatures, the Si/Ge atoms vibrate with a higher amplitude than the Ti and C atoms. These results reinforce the idea that Si and Ge act as rattlers, which, in turn, is believed to be responsible for the low phonon conductivities exhibited by these solids, despite high Young's moduli and Debye temperatures.

Intriguingly, the thermal expansions and isotropic thermal motion behavior do not differ significantly between these two isostructural phases. However, the anisotropic thermal motions, interatomic distances, and bond angles show strikingly different behavior. This surprising difference is tentatively explained to be a result of (i) the *anisotropic* motion of the Ge atoms parallel to the basal planes and (ii) their *correlated* motion with the Ti atoms.

The volume expansions calculated from HTND are $9.0(\pm0.1)\times10^{-6}$ K^{-1} and $8.7(\pm0.1)\times10^{-6}$ K^{-1} for Ti_3SiC_2 and Ti_3GeC_2, respectively; the expansions along the *a* and *c* axes are $\alpha_a=8.9(\pm0.1)\times10^{-6}$ K^{-1} and $\alpha_c=9.4(\pm0.1)\times10^{-6}$ K^{-1} for Ti_3SiC_2 and $\alpha_a=8.5(\pm0.1)\times10^{-6}$ K^{-1} and $\alpha_c=9.2((\pm0.1)\times10^{-6}$ K^{-1} for Ti_3GeC_2. Discontinuity in thermal motion results of the Ti_{II} atoms in Ti_3GeC_2 was observed between 300 and 500 °C during both heating and cooling, which may be related to the high mechanical damping observed previously in Ti_3GeC_2 at ≈427 °C.

ACKNOWLEDGMENTS

This work has benefited from the use of the Lujan Neutron Scattering Center at LANSCE, which is funded by the U.S. Department of Energy's Office of Basic Energy Sciences. Los Alamos National Laboratory is operated by Los Alamos National Security LLC under DOE Contract No. DE-AC52-06NA25396. This work was also partially funded by Graduate Assistance in Areas of National Need for Drexel Research and Education in Advanced Materials (GAANN-DREAM) under the U.S. Department of Education Grant No. P200A060117 and the Ceramics Division of the National Science Foundation (Grant No. DMR 0503711). M.W.B. would also like to acknowledge the financial support of the Wheatley Scholar of the Lujan Center at Los Alamos National Laboratory, which is funded by the Department of Energy's Office of Basic Energy Sciences under DOE Contract No. DE-AC52-06NA25396.

[1] M. W. Barsoum, Prog. Solid State Chem. **28**, 201 (2000).
[2] M. W. Barsoum and T. El-Raghy, J. Am. Ceram. Soc. **79**, 1953 (1996).
[3] T. El-Raghy, A. Zavaliangos, M. W. Barsoum, and S. R. Kalidindi, J. Am. Ceram. Soc. **80**, 513 (1997).
[4] M. W. Barsoum, T. El-Raghy, and L. U. J. T. Ogbuji, J. Electrochem. Soc. **144**, 2508 (1997).
[5] M. W. Barsoum and T. El-Raghy, J. Mater. Synth. Process. **5**, 197 (1997).
[6] A. Ganguly, T. Zhen, and M. W. Barsoum, J. Alloys Compd. **376**, 287 (2004).
[7] M. Radovic, M. W. Barsoum, T. El-Raghy, and S. Wiederhorn, Acta Mater. **49**, 4103 (2001).
[8] M. Radovic, M. W. Barsoum, T. El-Raghy, and S. M. Wiederhorn, J. Alloys Compd. **361**, 299 (2003).
[9] T. Zhen, M. W. Barsoum, S. R. Kalidindi, M. Radovic, Z. M. Sun, and T. El-Raghy, Acta Mater. **53**, 4963 (2005).
[10] W. Jeitschko and H. Nowotny, Monatsch. Chem. **98**, 329 (1967).
[11] H. Wolfsgruber, H. Nowotny, and F. Benesovsky, Monatsch. Chem. **98**, 2403 (1967).
[12] M. W. Barsoum, D. Brodkin, and T. ElRaghy, Scr. Mater. **36**, 535 (1997).
[13] S. Arunajatesan and A. H. Carim, Mater. Lett. **20**, 319 (1994).
[14] E. H. Kisi, J. A. A. Crossley, S. Myhra, and M. W. Barsoum, J. Phys. Chem. Solids **59**, 1437 (1998).
[15] M. W. Barsoum, T. El-Raghy, C. J. Rawn, W. D. Porter, H. Wang, E. A. Payzant, and C. R. Hubbard, J. Phys. Chem. Solids **60**, 429 (1999).
[16] M. Y. Gamarnik and M. W. Barsoum, J. Mater. Sci. **34**, 169 (1999).
[17] Y. C. Zhou and Z. M. Sun, J. Appl. Phys. **86**, 1430 (1999).
[18] P. Finkel, B. Seaman, K. Harrell, J. Palma, J. D. Hettinger, S. E. Lofland, A. Ganguly, M. W. Barsoum, Z. Sun, S. Li, and R. Ahuja, Phys. Rev. B **70**, 085104 (2004).
[19] M. K. Drulis, A. Czopnik, H. Drulis, J. E. Spanier, A. Ganguly, and M. W. Barsoum, Mater. Sci. Eng., B **119**, 159 (2005).
[20] T. H. Scabarozi, S. Amini, O. Leaffer, A. Ganguly, S. Gupta, W. Tambussi, S. Clipper, J. E. Spanier, M. W. Barsoum, J. D. Hettinger, and S. E. Lofland, J. Appl. Phys. **105**, 013543 (2009).
[21] M. Radovic, M. W. Barsoum, A. Ganguly, T. Zhen, P. Finkel, S. R. Kalidindi, and E. Lara-Curzio, Acta Mater. **54**, 2757 (2006).
[22] T. El-Raghy and M. W. Barsoum, J. Am. Ceram. Soc. **82**, 2849 (1999).
[23] H. R. Wenk, L. Lutterotti, and S. Vogel, Nucl. Instrum. Methods Phys. Res. A **515**, 575 (2003).
[24] S. C. Vogel, C. Hartig, L. Lutterotti, R. B. Von Dreele, H. R. Wenk, and D. J. Williams, Powder Diffr. **19**, 65 (2004).
[25] A. C. Larson and R. B. V. Dreele, General Structure Analysis System (GSAS), Los Alamos National Laboratory Report LAUR 86-748, 2004.
[26] L. Lutterotti, S. Matthies, H. R. Wenk, A. S. Schultz, and J. W. Richardson, J. Appl. Phys. **81**, 594 (1997).
[27] Y. Wang and J. C. Huang, Mater. Chem. Phys. **81**, 11 (2003).
[28] S. Matthies, J. Pehl, H. R. Wenk, L. Lutterotti, and S. C. Vogel, J. Appl. Crystallogr. **38**, 462 (2005).
[29] B. H. Toby, Powder Diffr. **21**, 67 (2006).
[30] C. R. Houska, J. Phys. Chem. Solids **25**, 359 (1964).
[31] C. J. Glassbrenner and G. A. Slack, Phys. Rev. **134**, A1058 (1964).
[32] V. Schomaker and R. E. Marsh, Acta Crystallogr., Sect. A: Found. Crystallogr. **39**, 819 (1983).
[33] D. C. Palmer, C. S. Ltd., Bicester, Oxfordshire, UK, 2009.
[34] Y. C. Zhou, Z. M. Sun, X. H. Wang, and S. Q. Chen, J. Phys.: Condens. Matter **13**, 10001 (2001).
[35] W. Jeitschko, H. Nowotny, and F. Benesovsky, Monatsch. Chem. **94**, 672 (1963).
[36] H. X. Yang, B. Manoun, R. T. Downs, A. Ganguly, and M. W. Barsoum, J. Phys. Chem. Solids **67**, 2512 (2006).
[37] H. O. Pierson, *Handbook of Refractory Carbides and Nitrides* (Noyes, Westwood, NJ, 1996).
[38] A. Togo, L. Chaput, I. Tanaka, and G. Hug, Phys. Rev. B **81**, 174301 (2010).
[39] M. G. Tucker, M. T. Dove, and D. A. Keen, J. Phys.: Condens. Matter **12**, L425 (2000).
[40] M. W. Barsoum, C. J. Rawn, T. El-Raghy, A. T. Procopio, W. D. Porter, H. Wang, and C. R. Hubbard, J. Appl. Phys. **87**, 8407 (2000).